Highly localized quasiatomic minimal basis orbitals for Mo from *ab initio* calculations

T.-L. Chan,[1] Y. X. Yao,[1] C. Z. Wang,[1] W. C. Lu,[1] J. Li,[2] X. F. Qian,[3] S. Yip,[3] and K. M. Ho[1]
[1]*Ames Laboratory-U.S. DOE. and Department of Physics and Astronomy, Iowa State University, Ames, Iowa 50011, USA*
[2]*Department of Materials Science and Engineering, Ohio State University, Columbus, Ohio 43210, USA*
[3]*Department of Nuclear Science and Engineering, Massachusetts Institute of Technology, Cambridge, Massachusetts 02139, USA*
(Received 26 January 2006; revised manuscript received 3 July 2007; published 28 November 2007)

A minimal basis set of localized quasiatomic orbitals for Mo is constructed using the fully converged eigenstates from first-principles calculations with a large basis set. The orbitals, although similar in shape to those of a free atom, are slightly deformed such that it can reproduce all the occupied-state electronic properties of the system. They are very useful for analyzing chemical bonding by calculating the Mulliken overlap population and bond order index between atoms. In addition, the transferability of tight-binding parametrizations can be evaluated, for example, the effect of the two-center approximation.

DOI: 10.1103/PhysRevB.76.205119 PACS number(s): 71.20.−b, 71.15.Ap

I. INTRODUCTION

The electronic structures of periodic systems in solid-state physics are usually formulated in the reciprocal space. While it is technically elegant and simple to implement computationally, the formalism lacks in providing an easy connection to traditional chemical concepts with an intuitive picture about the bonding properties of crystal in real space. Hence, a representation using localized orbitals is appealing and also important for modern theories of electron correlations[1] and electron polarization.[2,3] Moreover, localized orbitals play a key role in the development of $O(N)$ methods,[4–8] where the computational effort of electronic structure calculations scales linearly with the system size.

Wannier functions (WFs), introduced by Wannier in 1937,[9] are the most widely used functions to describe the electronic structures of crystals in real space. Since WFs are constructed by a unitary transformation of the canonical electronic eigenstates of the crystal, they cover the same space as that spanned by the eigenstates from which the WFs are constructed. However, well-localized WFs exist only in large-gap insulators but not in metallic systems.[10,11] A lot of effort has been focused on obtaining maximally localized generalized WFs.[12–16] In particular, Souza *et al.* have shown that it is possible to generate atomiclike Wannier orbitals by including a suitable number of unoccupied bands in addition to the occupied bands.[16] Recently, we proposed a new scheme to construct highly localized quasiatomic minimal basis orbitals (QUAMBOs)[17] for both insulating and metallic systems, using the electronic eigenstates obtained from first-principles calculations. Our scheme selects a relevant subset of antibonding states from a large unoccupied subspace. The antibonding states are chosen to maximize the localization of the resulting QUAMBOs. The QUAMBOs contain the adaptation of the minimal basis to the environment and reproduce exactly the first-principles electronic structures of the occupied states. Previously, we have successfully constructed QUAMBOs for Si and Al in diamond and fcc structures resulting in highly localized s- and p-like orbitals. In this paper, we will demonstrate that the algorithm can be applied to transition metals as well. bcc-Mo is chosen as our prototype system in this study. QUAMBOs of fcc-Mo are also calculated to compare the bonding between bcc and fcc structures. We will also use the QUAMBOs to examine the transferability of tight-binding models based on the two-center approximation and find out whether electronic structures can be accurately reproduced under such tight-binding scheme. The construction of QUAMBOs can be done under the scheme of Vanderbilt's ultrasoft pseudopotentials[18] or Blochl's projector augmented-wave[19] method and will be described elsewhere.[20]

II. FORMALISM AND ALGORITHM FOR QUASIATOMIC MINIMAL BASIS ORBITAL CONSTRUCTION

Given a set of Bloch eigenstates $\phi_{\mathbf{k},\mu}(\mathbf{r})$ obtained from first-principles calculations using a large basis set, with the eigenstates being labeled by the wave vector $\mathbf{k}$ in the Brillouin zone and the band number μ, we want to construct a set of quasiatomic orbitals $A_\alpha(\mathbf{r}-\mathbf{R}_i)$ $[|A_\alpha(\mathbf{R}_i)\rangle$ in bra-ket notation] for each atom i at position $\mathbf{R}_i$ in the unit cell and for each orbital type α (s,p_x,p_y,p_z, etc.) by linear combinations of the Bloch eigenstates. For each wave vector $\mathbf{k}$, a total of n_{tot} bands are calculated, with $n_{occ}(\mathbf{k})$ of them being occupied and the rest $n_{vir}(\mathbf{k})$ are unoccupied. However, only a subspace of the unoccupied bands is needed and this subspace should be optimized in order to enhance the localization of the QUAMBOs when combined coherently with the occupied bands. This optimal subset of virtual bands $\phi_{\mathbf{k},p}(\mathbf{r})$ is obtained by a linear transformation,

$$\phi_{\mathbf{k},p}(\mathbf{r}) = \sum_{\mu=n_{occ}+1}^{n_{tot}} T_{\mu p}(\mathbf{k})\phi_{\mathbf{k},\mu}(\mathbf{r}), \quad p = 1,2,\ldots,n_p(\mathbf{k}) < n_{vir}(\mathbf{k}), \tag{1}$$

where T is a rectangular matrix to be determined later, which satisfies $T\cdot T^\dagger = I$ since $\phi_{\mathbf{k},p}(\mathbf{r})$ is an orthogonal set. The quasiatomic orbitals can be constructed by a linear combination of the occupied bands and the optimized virtual bands,

$$A_\alpha(\mathbf{r}-\mathbf{R}_i)=\sum_{\mathbf{k}}\left[\sum_{\mu=1}^{n_{occ}} a_{\mu\alpha}(\mathbf{k},\mathbf{R}_i)\phi_{\mathbf{k},\mu}(\mathbf{r}) + \sum_{p=1}^{n_p} b_{p\alpha}(\mathbf{k},\mathbf{R}_i)\phi_{\mathbf{k},p}(\mathbf{r})\right]. \quad (2)$$

We require each A_α to be as close as possible to its corresponding free-atom orbital A_α^0. The minimization of the mean square deviation $\langle A_\alpha - A_\alpha^0 | A_\alpha - A_\alpha^0\rangle$ under the norm-conserving constraint $\langle A_\alpha | A_\alpha\rangle = 1$ yields

$$A_\alpha(\mathbf{r}-\mathbf{R}_i)=D_{i\alpha}^{-1/2}\left\{\sum_{\mathbf{k}}\left[\sum_{\mu=1}^{n_{occ}}\langle\phi_{\mathbf{k},\mu}|A_\alpha^0(\mathbf{R}_i)\rangle\phi_{\mathbf{k},\mu}(\mathbf{r}) + \sum_{p=1}^{n_p}\langle\phi_{\mathbf{k},p}|A_\alpha^0(\mathbf{R}_i)\rangle\phi_{\mathbf{k},p}(\mathbf{r})\right]\right\}, \quad (3)$$

where

$$D_{i\alpha}(\mathbf{R}_i)=\sum_{\mathbf{k}}\left[\sum_{\mu=1}^{n_{occ}}|\langle\phi_{\mathbf{k},\mu}|A_\alpha^0(\mathbf{R}_i)\rangle|^2+\sum_{p=1}^{n_p}|\langle\phi_{\mathbf{k},p}|A_\alpha^0(\mathbf{R}_i)\rangle|^2\right] \quad (4)$$

and is related to the root-mean-square deviation of the optimized A_α from the corresponding free atom A_α^0 by

$$\Delta_{i\alpha}=\langle A_\alpha - A_\alpha^0 | A_\alpha - A_\alpha^0\rangle^{1/2}=[2(1-D_{i\alpha}^{1/2})]^{1/2}. \quad (5)$$

Equation (5) suggests that the key step to obtaining quasiatomic localized orbitals is to select a virtual band subset $\phi_{\mathbf{k},p}(\mathbf{r})$ that maximizes the sum $\Sigma_{i,\alpha}D_{i\alpha}$, i.e., maximizing the overall overlap between the virtual bands and the free-atom orbitals. With the subset of virtual bands chosen according to this criteria (details to be given below), QUAMBOs can be constructed through Eq. (3). The step-by-step algorithm for constructing the QUAMBOs for Mo is described as follows.

A. Calculation of Bloch eigenstates from first-principles calculations

First, the electronic eigenstates of Mo in bcc structure are calculated using first-principles density functional theory under local density approximation (LDA).[21] The Kohn-Sham equations are solved self-consistently using pseudopotential[22] with a mixed basis of plane waves and Gaussian functions[23] to enable adequate convergence for the localized *d*-like orbitals. The cutoff energy is set to be 40 Ry and a Monkhorst-Pack grid[24] of $16\times16\times16$ is used for the Brillouin zone integration. A total of 70 bands are calculated for each **k** point in our grid.

B. Projection of Bloch eigenstates onto free-atom orbitals

In our QUAMBO construction, we need to project the Bloch eigenstates obtained from previous *ab initio* calculations onto the free-atom orbitals [see Eqs. (3) and (4)]. We choose the 5*s* and 4*d* pseudo-wave-functions as our free-atom orbitals A_α^0. The pseudo-wave-functions are constrained to match the corresponding ground state wave functions of a free Mo atom exactly outside a core radius and reproduce the atomic energy levels at the same time. The radial part of the pseudo-wave-functions is designed to be nodeless inside the core radius that joins smoothly to the wave function outside the core, and the integrated charge of the pseudo-wave-functions is required to be normalized. Six QUAMBOs per Mo atom will be generated to maximize the overlap with these six free-atom orbitals $A_\alpha^0(\alpha = s, d_{xy}, d_{yz}, d_{zx}, d_{x^2-y^2}, d_{3z^2-r^2})$. In order to calculate the projection $\langle\phi_{\mathbf{k},\mu}|A_\alpha^0(\mathbf{R}_i)\rangle$, the Bloch eigenstates $\phi_{\mathbf{k},\mu}(\mathbf{r})$ originally given by a mixed basis of plane waves and Gaussian functions are now reexpressed using plane waves with a cutoff energy of 80 Ry; this is because integration involving plane waves is computationally simpler. We checked that the plane wave set is large enough that our study following the QUAMBO construction, for example, bonding analysis in the following sections, is converged. It should be noted that *p* orbitals are not included in the construction. We found that six *s*- and *d*-like QUAMBOs are sufficient to serve as a minimal basis set that reproduces the properties of Mo in a bcc crystal.

C. Determination of the virtual subspace

By virtue of Eq. (4) and the orthonormality of the virtual subset, the optimization of the virtual bands can be done by diagonalizing the matrix

$$B_{\mu\mu'}^{\mathbf{k}}=\sum_{i,\alpha}\langle\phi_{\mathbf{k},\mu}|A_\alpha^0(\mathbf{R}_i)\rangle\langle A_\alpha^0(\mathbf{R}_i)|\phi_{\mathbf{k},\mu'}\rangle, \quad (6)$$

for each **k** point, where μ and μ' run over all the unoccupied states obtained in our first-principles calculation. The subset of eigenvectors of the *B* matrix defines the transformation matrix *T* in Eq. (1) for optimizing the virtual bands. The eigenvalues and eigenvectors are ranked in descending order with the largest eigenvalues being the first one. Hence, after the transformation, the virtual space for each **k** point will have the first virtual state giving the largest overlap with the free-atom orbitals A_α^0, and the second virtual state having the second largest overlap and so on.

A Bloch wave function for the QUAMBOs can be obtained by

$$\tilde{A}_{\mathbf{k},\alpha}(\mathbf{r}-\mathbf{R}_i)=D_{i\alpha}^{-1/2}\left[\sum_{\mu=1}^{n_{occ}}\langle\phi_{\mathbf{k},\mu}|A_\alpha^0(\mathbf{R}_i)\rangle\phi_{\mathbf{k},\mu}(\mathbf{r}) + \sum_{p=1}^{n_p}\langle\phi_{\mathbf{k},p}|A_\alpha^0(\mathbf{R}_i)\rangle\phi_{\mathbf{k},p}(\mathbf{r})\right], \quad (7)$$

analogous to Eq. (3). The size of the virtual subspace $n_p(\mathbf{k})$ is chosen such that the sum $n_{occ}(\mathbf{k})+n_p(\mathbf{k})$ is equal to the number of desired QUAMBOs. For Mo in bcc structure, there are only one atom in a unit cell and six QUAMBOs are being sought for this atom; hence, $n_p(\mathbf{k})=6-n_{occ}(\mathbf{k})$. The first n_p states from the virtual space will be chosen. Since the virtual states are ranked according to the amount of overlap with the free-atom orbitals, the chosen virtual subspace of size n_p provides the best "antibonding" states to combine with the occupied states to produce localized quasiatomic orbitals. In

this scheme, the transformation of occupied and virtual states to $\tilde{A}_{\mathbf{k},\alpha}$ has to be invertible and numerically stable. We found that if three additional p-like QUAMBOs are included, giving a total of nine QUAMBOs, the transformations become singular or badly conditioned no matter how the virtual subspace is being chosen. The matrices corresponding to the transformations from the nine occupied and virtual states to nine $\tilde{A}_{\mathbf{k},\alpha}$ are singular when there are rows in the matrices that are linearly dependent. This happens when the nine states do not span a nine dimensional space after projection onto the free-atom orbitals. This indicates that the six s- and d-like QUAMBOs already constitute a sufficient basis set to describe the system; extra QUAMBOs are redundant leading to singular transformations.[25] Since the transformation is required to be invertible, our QUAMBOs reproduce all the occupied eigenstates and eigenvalues of the system. However, for a metallic system such as Mo, it is preferable to preserve the electronic properties not only below the Fermi level but also slightly above the Fermi level as well. Hence, additional eigenstates up to 1 eV above the Fermi level are included into n_{occ}, with the construction of the virtual subspace obtained by higher unoccupied states rather than unoccupied states immediately above the Fermi level.

D. Construction of orthogonalized quasiatomic minimal basis orbitals

Once the set of $\tilde{A}_{\mathbf{k},\alpha}(\mathbf{r}-\mathbf{R}_i)$ has been determined through Eq. (7), the QUAMBOs can be constructed by summing up all the $\tilde{A}_{\mathbf{k},\alpha}(\mathbf{r}-\mathbf{R}_i)$ over the first Brillouin zone,

$$A_\alpha(\mathbf{r}-\mathbf{R}_i)=\sum_{\mathbf{k}}\tilde{A}_{\mathbf{k},\alpha}(\mathbf{r}-\mathbf{R}_i). \tag{8}$$

Although, in general, the QUAMBOs are not an orthogonal set by such a construction, the QUAMBOs belonging to the same atom can be orthogonalized by symmetric orthogonalization,

$$\hat{A}_\alpha(\mathbf{r}-\mathbf{R}_i)=\sum_{\alpha'}A_\alpha(\mathbf{r}-\mathbf{R}_i)(S^{-1/2})_{\alpha\alpha'}, \tag{9}$$

where $S_{\alpha\alpha'}=\langle A_\alpha(\mathbf{R}_i)|A_{\alpha'}(\mathbf{R}_i)\rangle$.

III. RESULTS AND DISCUSSIONS

A. Properties of the quasiatomic minimal basis orbitals

By following the recipe described above, the s- and d-like QUAMBOs for Mo in bcc structure are obtained and the results are displayed in Fig. 1. The corresponding contour plots are shown in Fig. 2 together with the s- and d-like QUAMBOs for fcc-Mo and the free-atom orbitals for comparison. Due to symmetry, $\hat{A}_{d_{xy}}$ and $\hat{A}_{d_{zx}}$ are not shown in the contour plots since they are the same as $\hat{A}_{d_{yz}}$ when projected onto the appropriate atomic plane. From Fig. 2, we can see that the bcc QUAMBOs are very similar to the corresponding orbitals in the free atom. The root-mean-square deviations ($\Delta_{i\alpha}$) between the bcc QUAMBOs and the corresponding free-atom orbitals are 16.4% for s-, 7.5% for d_{xy},d_{yz},d_{zx}-, and 7.0% for $d_{x^2-y^2}$, $d_{3z^2-r^2}$-like QUAMBOs, respectively. The deformation of the QUAMBOs is more pronounced along the bonds between the atoms. The QUAMBOs for fcc-Mo are also quite similar to the free-atom orbitals. Their deformation is different from the bcc QUAMBOs with deviations of 16.5% for s-, 7.2% for d_{xy},d_{yz},d_{zx}-, and 6.5% for $d_{x^2-y^2}$, $d_{3z^2-r^2}$-like QUAMBOs, respectively.

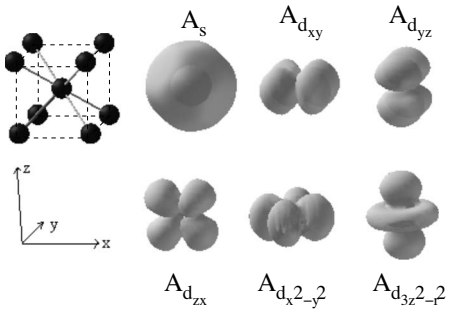

FIG. 1. Three-dimensional plots for the six QUAMBOs of Mo in bcc structure. A cubic unit cell of the bcc structure is also shown in the same scale as in the QUAMBO plot.

As explained above, the QUAMBOs are constructed such that they can reproduce the occupied-state electronic properties obtained from a first-principles calculation

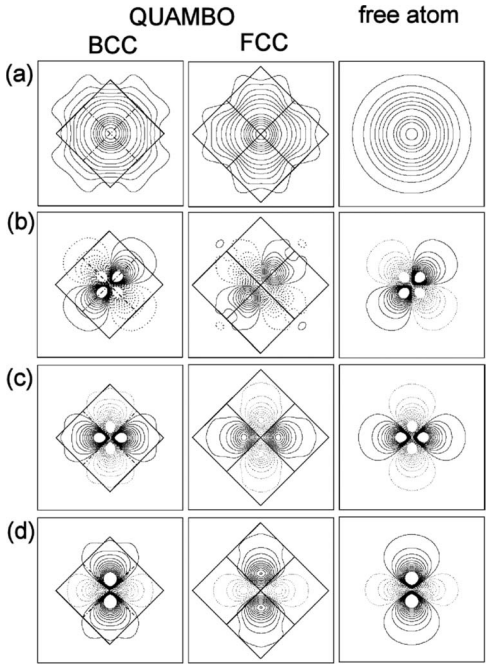

FIG. 2. Contour plot of the QUAMBOs of Mo in bcc structure shown in Fig. 1: (a) s-like, (b) d_{yz}-like, (c) $d_{x^2-y^2}$-like, and (d) $d_{3z^2-r^2}$-like QUAMBOs with their corresponding QUAMBOs of Mo in fcc structure and free-atom orbitals for comparison. (a), (b), and (d) are plotted in the (100) plane and (c) is plotted in the (001) plane. The solid and dotted contour lines have opposite sign. The outermost contour line has the value of 0.02 Å$^{-3/2}$. The contour step is 0.02 Å$^{-3/2}$ for (a) and 0.04 Å$^{-3/2}$ for (b)–(d). The two perpendicular lines passing through the center of the QUAMBOs indicate the directions of the nearest-neighbor atoms. If the nearest neighbors are out of the plane, the lines are drawn as dashed. The corners of the square indicate the positions of the second nearest neighbors.

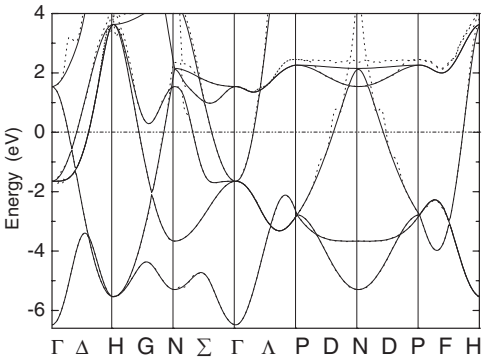

FIG. 3. Electronic band structure for bcc-Mo along symmetry directions calculated using a mixed-basis first-principles LDA method (solid line) and using QUAMBOs as a basis set (dotted line).

using a large basis set. This can be demonstrated explicitly by comparing the band structure and density of states of bcc-Mo calculated using QUAMBOs as bases with those obtained from our original LDA calculation. The matrix element of the Hamiltonian under QUAMBOs is $H_{\alpha\alpha'}(\mathbf{k})=\langle\tilde{A}_{\mathbf{k},\alpha}(\mathbf{R}_i)|H|\tilde{A}_{\mathbf{k},\alpha'}(\mathbf{R}_{i'})\rangle$, where $\tilde{A}_{\mathbf{k},\alpha}(\mathbf{r}-\mathbf{R}_i)=\frac{1}{\sqrt{N}}\Sigma_{\mathbf{R}_n}e^{i\mathbf{k}\cdot\mathbf{R}_n}\hat{A}_\alpha(\mathbf{r}-\mathbf{R}_i-\mathbf{R}_n)$ is the Bloch sum of the QUAMBO $\hat{A}_\alpha(\mathbf{r}-\mathbf{R}_i)$, $\mathbf{k}$ is an arbitrary $\mathbf{k}$ point in the Brillouin zone not restricted to those in the $\mathbf{k}$-point grid from our first-principles calculation, and $\mathbf{R}_n$ are the lattice vectors of the bcc crystal structure. The total Hamiltonian $H=\Sigma_{\mathbf{k}'}\Sigma_{\mu=1}^{n_{tot}}|\phi_{\mathbf{k}',\mu}\rangle E_{\mathbf{k}',\mu}\langle\phi_{\mathbf{k}',\mu}|$ when expressed using the eigenstates of the system. Here, $\mathbf{k}'$ runs over the $\mathbf{k}$-point grid chosen for the Brillouin zone integration in our first-principles calculation. It is straightforward to show that

$$H_{\alpha\alpha'}(\mathbf{k})=\sum_{\mathbf{R}_n}\langle\hat{A}_\alpha(\mathbf{R}_i)|H|\hat{A}_{,\alpha'}(\mathbf{R}_{i'}+\mathbf{R}_n)\rangle e^{i\mathbf{k}\cdot\mathbf{R}_n}$$
$$=\sum_{\mathbf{R}_n}\sum_{\mathbf{k}'}H_{\alpha\alpha'}(\mathbf{k}')e^{i(\mathbf{k}-\mathbf{k}')\cdot\mathbf{R}_n}. \quad (10)$$

Using Eq. (10), the Hamiltonian can be calculated at any $\mathbf{k}$ point with the QUAMBOs as bases. Since the QUAMBOs do not form an orthogonal set, the band structure is obtained by solving a generalized eigenvalue problem. The band structure along the symmetry directions of the Brillouin zone is shown in Fig. 3. When compared with the original LDA calculation, we can see that the eigenvalues are exactly reproduced at the $\mathbf{k}$-point grid used in the first-principles calculation up to 1 eV above the Fermi level. Outside of the $\mathbf{k}$-point grid, slight discrepancy in the band structure can be found between the first-principles results and that from QUAMBOs. This discrepancy can be minimized by using a finer $\mathbf{k}$-point grid in the first-principles calculation to construct the QUAMBOs.

The result for the density of states is shown in Fig. 4(a). The density of states is well reproduced up to 1 eV above the Fermi level. It should be noted that the same method of constructing QUAMBOs for Al resulted in an energy gap opening up immediately at the energy where the forced reproduction of the eigenstates terminates,[17] but this situation does not occur for Mo, as shown in Fig. 4. This probably implies that the QUAMBOs for Mo are not too bad a representation for the space even beyond 1 eV above the Fermi level, although it will not be exact. In addition, the projected density of states into *s* and *d* contribution is shown in Fig. 4(b). When compared to the usual method by projecting the eigenstates onto spherical harmonics in atomic spheres centered at the respective ions' positions, QUAMBOs produce the same result qualitatively. However, QUAMBOs do not rely on an *ad hoc* definition of atomic spheres that either cannot fill the whole space, resulting in a loss of electron, or overlap, leading to double counting from the overlapping

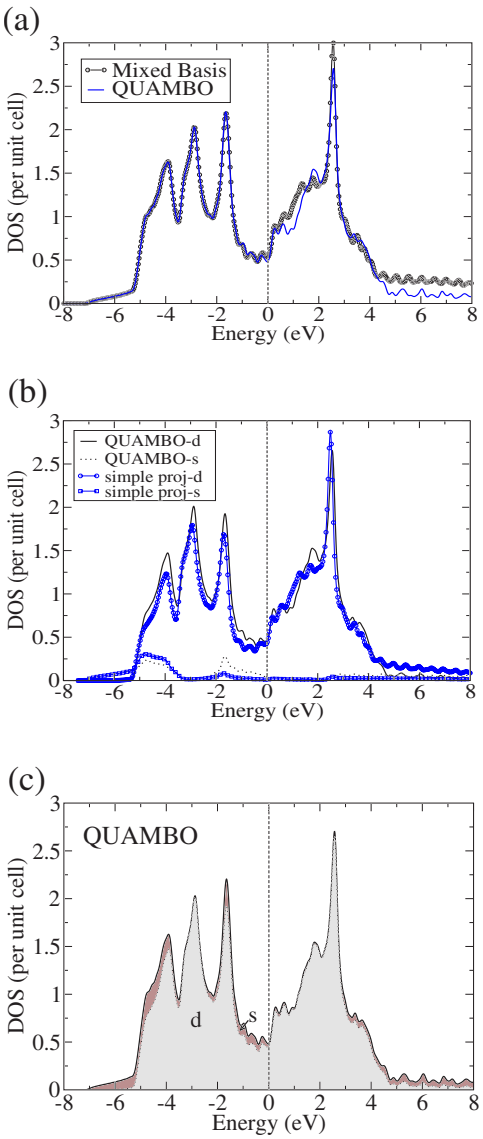

FIG. 4. (Color online) (a) Electronic density of states of bcc-Mo obtained by using QUAMBOs as a basis set, compared with those from the original mixed-basis first-principles LDA calculations. (b) Projected density of states into *s* and *d* components by using QUAMBOs as a basis set and by simple projection (projecting the eigenstates onto spherical harmonics in atomic spheres). (c) Projected density of states using QUAMBOs illustrating the *s* and *d* contribution add up to the total density of states.

regions. Since the occupied eigenstates can be exactly decomposed into Bloch functions of QUAMBOs localized on different atoms and angular momentum channels as discussed in the previous session, the *s* and *d* contribution of the density of states can indeed add up to give the total density of states, as depicted in Fig. 4(c).

B. Chemical bonding analysis based on the quasiatomic minimal basis orbitals

The occupied eigenstates $\phi_{\mathbf{k},\mu}(\mathbf{r})$ from our first-principles calculations can be expressed in terms of Bloch sums of QUAMBOs $\tilde{A}_{\mathbf{k},\alpha}$ as $\phi_{\mathbf{k},\mu}=\Sigma_{i,\alpha}c_{\mu,\alpha}(\mathbf{k},\mathbf{R}_i)\tilde{A}_{\mathbf{k},\alpha}(\mathbf{r}-\mathbf{R}_i)$. The Mulliken overlap population matrix[26] between the *i*th atom of the origin cell and the *j*th atom of cell $\mathbf{R}_n$ is then defined as

$$M_{i0,jn}=N^{-1}\sum_{k,\alpha,\beta}P^{i,j}_{\alpha,\beta}(\mathbf{k})S^{jn,i0}_{\beta,\alpha}(\mathbf{k}), \tag{11}$$

where $P^{i,j}_{\alpha,\beta}(\mathbf{k})=\Sigma^{n_{occ}}_{\mu}2c_{\mu,\alpha}(\mathbf{k},\mathbf{R}_i)c^{*}_{\mu,\beta}(\mathbf{k},\mathbf{R}_j)$ and $S^{jn,i0}_{\beta,\alpha}(\mathbf{k})=\langle\hat{A}_{\beta}(\mathbf{R}_j+\mathbf{R}_n)|\hat{A}_{\alpha}(\mathbf{R}_i)\rangle e^{i\mathbf{k}\cdot\mathbf{R}_n}$. $M_{i0,jn}$ is the partial trace of a density matrix (PS), which is expressed under a nonorthogonal basis set (because QUAMBOs between different atoms are not orthogonalized) in reciprocal space. The trace sums over all the orbitals of the *i*th atom of the origin cell and the *j*th atom of cell $\mathbf{R}_n$. In a similar way, the bond order index[27] for a system without spin polarization can be expressed as

$$\mathrm{BO}_{i0,jn}=\sum_{\alpha\in i0,\beta\in jn}(PS)^{i0,jn}_{\alpha\beta}(PS)^{jn,i0}_{\beta\alpha}, \tag{12}$$

where $(PS)^{i0,jn}_{\alpha\beta}=N^{-1}\Sigma_{\mathbf{k}}[P(\mathbf{k})\cdot S(\mathbf{k})]_{\alpha\beta}e^{-i\mathbf{k}\cdot\mathbf{R}_n}$ with $S^{j,i}_{\beta\alpha}(\mathbf{k})=\langle\tilde{A}_{\mathbf{k},\beta}|\tilde{A}_{\mathbf{k},\alpha}\rangle=\Sigma_m S^{jm,i0}_{\beta,\alpha}(\mathbf{k})$. The bond order between the two atoms is the trace of the square of the density matrix with the trace summing over the orbitals of the two atoms.

Based on Eqs. (11) and (12), we compared the matrix elements $M_{i0,jn}$ and the bond order indices $\mathrm{BO}_{i0,jn}$ for bcc-Mo and fcc-Mo in Fig. 5. The Mulliken overlap populations are two times $M_{i0,jn}$. The overlap population and bond order are concentrated on the first and second neighbors. Both $M_{i0,jn}$ and $\mathrm{BO}_{i0,jn}$ have higher magnitudes for Mo in bcc structure than in fcc; this is because each atom in the fcc structure has 12 nearest neighbors compared to 8 in bcc; hence, each individual bond is weaker in fcc. To further our understanding of the nature of bonding in Mo crystal, we decompose the matrix elements $M_{i0,jn}$ into contribution from the overlap between different orbitals. The decomposed matrix elements between the origin atom and an atom in the first neighbor $[(1/2,1/2,-1/2)a$ for bcc and $(1/2,0,1/2)a$ for fcc, where *a* is the lattice constant$]$ $M_{0,1}$ are shown in Table I; the indices *i* and *j* are omitted for clarity because there is only one atom in the primitive unit cell for both bcc and fcc structures. For bcc-Mo, we can see that the ss-σ bond accounts for nearly 20% of $M_{0,1}$. On the other hand, $d_{zx}d_{zx}$ $-\sigma$ and $-\delta$ bonds account for more than 25% of $M_{0,1}$ in the fcc structure. This difference can be understood by the close-packed nature of the fcc structure, which promotes bonding between the localized *d* electrons in Mo, while the ss-σ bonding is more convenient for a slightly more open structure as in bcc. For the matrix element between the origin atom and the second neighbors, the ss-σ antibonding dominates $M_{0,2}$ for both fcc and bcc structures. The ss-σ bond contributes 80% and 70% to $M_{0,2}$ in bcc and fcc structures, respectively.

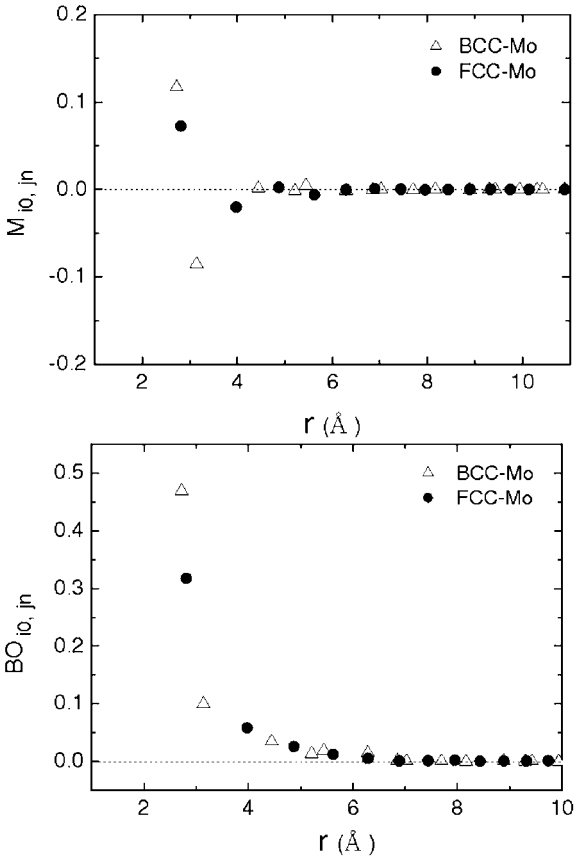

FIG. 5. The matrix elements $M_{i0,jn}$ (top) and bond order index $\mathrm{BO}_{i0,jn}$ (bottom) between the origin atom and its various neighbors for Mo in bcc and fcc structures.

In Fig. 6, our results for $M_{i0,jn}$ as a function of the interatomic distances of bcc-Mo are plotted together with those of diamond-Si and fcc-Al structures from our previous study[17] for comparison. The overlap populations of both Si and Mo extend only up to the second neighbors, while the overlap populations of fcc-Al are smaller for the first neighbor but extend up to the fifth neighbors, reflecting the diffuse nature of the bonding in Al.

C. Analysis of tight-binding hopping and overlap matrix elements

Tight-binding electronic calculations under the Slater-Koster scheme[28] have been widely employed to provide interatomic forces for the molecular dynamics simulation of materials. In this scheme, a fixed minimal basis set and two-center approximation are used to simplify the quantum me-

TABLE I. The first-neighbor overlap population matrix elements for bcc- and fcc-Mo decomposed into overlaps between different orbitals. The matrix elements are calculated between the atom at the origin and an atom in the first neighbor: $(1/2,1/2,-1/2)a$ for bcc and $(1/2,0,1/2)a$ for fcc. Only the diagonal and upper triangle are shown because the array is symmetric.

$M_{0,1}$	s	d_{xy}	d_{yz}	d_{zx}	$d_{x^2-y^2}$	$d_{3z^2-r^2}$
			bcc			
s	0.02114	−0.00105	−0.00105	−0.00105	0	0
d_{xy}		0.00278	0.00451	0.00451	0	0.00827
d_{yz}			0.00278	0.00451	0.0062	0.00207
d_{zx}				0.00278	0.0062	0.00207
$d_{x^2-y^2}$					0.00846	0
$d_{3z^2-r^2}$						0.00846
			fcc			
s	0.00287	0	0	0.00352	0.00191	0.00064
d_{xy}		0.00084	0.00685	0	0	0
d_{yz}			0.00084	0	0	0
d_{zx}				0.01940	0.00237	0.00079
$d_{x^2-y^2}$					0.00053	0.00795
$d_{3z^2-r^2}$						0.00584

chanical calculations. A fixed minimal basis set means that the basis is not allowed to vary according to the bonding environment. The two-center approximation assumes that the potentials from the atoms other than the pair of atoms for which the Hamiltonian matrix elements are evaluated can be neglected. There is a question of whether such simplifications will affect the transferability of the tight-binding potentials, hence limiting their accuracy in predicting electronic structures under different bonding environments. As illustrated above, QUAMBOs as a minimal basis set must deform to adapt to the changes of the bonding environment in order to reproduce all the occupied electronic state properties. In this subsection, we will evaluate the validity of the two-center approximation for Mo and provide insights on improving the parametrization of the tight-binding models.

In tight-binding models, the electronic structures are obtained by solving the following generalized eigenvalue problem:

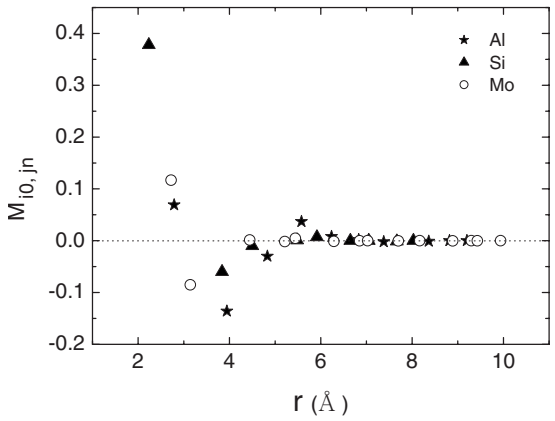

FIG. 6. The matrix elements $M_{i0,jn}$ between the origin atom and its various neighbors for diamond-Si, fcc-Al, and bcc-Mo.

$$H|\phi_{k,n}\rangle = \epsilon_{k,n}S|\phi_{k,n}\rangle, \tag{13}$$

in which $|\phi_{k,n}\rangle$ is a linear combination of the Bloch wave function of atomiclike orbitals localized at atomic position $\mathbf{R}_i$ with angular momentum α, i.e., $|\phi_{k,n}\rangle = \Sigma_{i,\alpha} C_{k,n,i,\alpha} N^{-1/2} \Sigma_{\mathbf{R}_i} A_\alpha(\mathbf{r}-\mathbf{R}_i) e^{i\mathbf{k}\cdot\mathbf{R}_i}$. Hence, the Hamiltonian and overlap matrix elements in the QUAMBO representation can be obtained by evaluating the hopping integrals $\langle A_\alpha(\mathbf{R}_i)|H|A_{\alpha'}(\mathbf{R}_{i'})\rangle$ and the overlap integrals $S_{\alpha i,\alpha' i'} = \langle A_\alpha(\mathbf{R}_i)|A_{\alpha'}(\mathbf{R}_{i'})\rangle$ between different orbitals used in the basis set. Under the Slater-Koster scheme, the Hamiltonian and overlap matrix elements can be further decomposed into different angular momentum components using the two-center approximation. For Mo with s and d orbitals, the hopping and overlap integrals can be decomposed into $ss\sigma$-, $sd\sigma$-, $dd\sigma$-, $dd\pi$-, and $dd\delta$-like components. By using the QUAMBOs constructed above as our basis set, we calculated the overlap and hopping matrix elements for different crystal structures as a function of interatomic distance and decompose them into the two-center Slater-Koster hopping and overlap integrals. The extraction of $ss\sigma$-, $sd\sigma$-, $dd\sigma$-, $dd\pi$-, and $dd\delta$-like components is not unique; it depends on which neighboring atom and which Hamiltonian matrix elements we use. This is an evidence that the two-center approximation is not adequate. Nevertheless, the Slater-Koster integrals are obtained using least-squares fitting, and the standard deviation of the data points in the hopping integrals is found to be less than 0.05 eV. The results are plotted in Figs. 7 and 8.

Since the QUAMBOs are deformed according to different bonding environments, it is expected that the overlap integrals can vary for different crystal structures. However, from Fig. 7, the overlap integrals corresponding to different structures fall onto the same curve very nicely. On the contrary, the hopping integrals in Fig. 8 are obviously not just a function of interatomic distance but also depend on the bonding

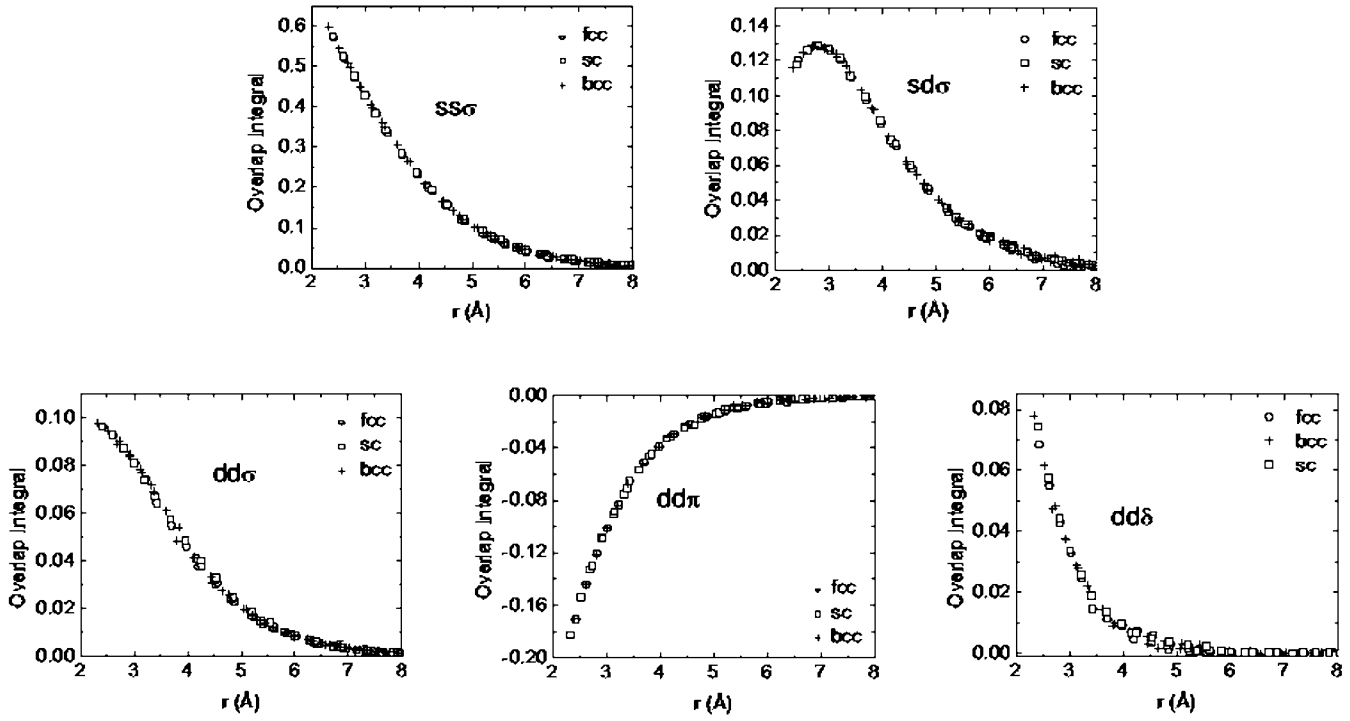

FIG. 7. Overlap integrals as a function of interatomic distance for Mo in the bcc, fcc, and sc structures decomposed under the Slater-Koster tight-binding scheme.

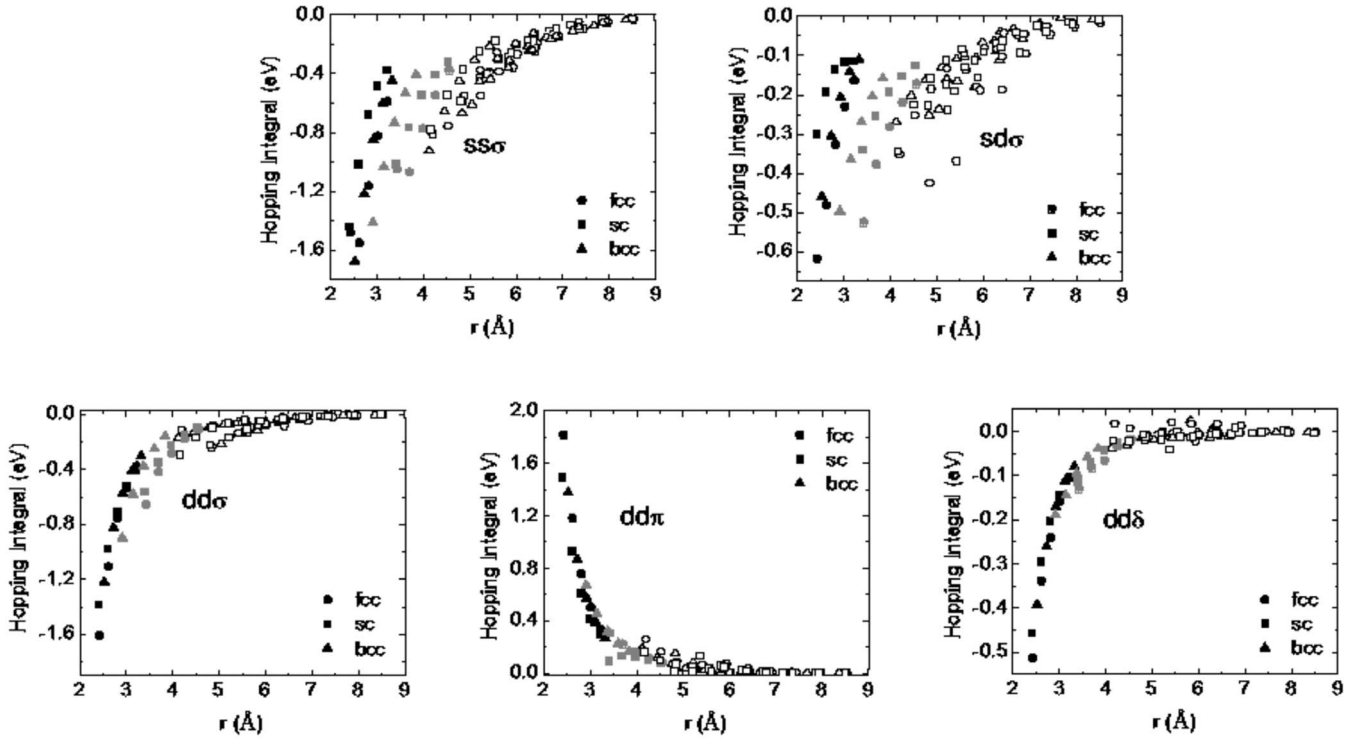

FIG. 8. Nonorthogonal hopping integrals for Mo as a function of interatomic distance in the bcc, fcc, and sc structures decomposed under the Slater-Koster tight-binding scheme. The black (gray) data points correspond to hopping integrals extracted from nearest (second nearest) neighbors, while the unshaded points correspond to third and further neighbors.

environment. Specifically, the hopping integrals calculated from simple cubic (sc), fcc, and bcc crystal structures are all different even if the distance between the pair of atoms is the same. In addition, there are discontinuities in the curves when the hopping integrals are extracted from the next-nearest-neighbor atoms as the interatomic distance increases. For example, the hopping integrals extracted from the second nearest neighbors in a compressed crystal structure are different from that of the nearest neighbors at the same interatomic distance. This is due to the screening from the nearest neighbors modifying the hopping to the second neighbors. We can also observe that the spread of hopping integrals due to different crystal structures is much larger for $ss\sigma$ and $sd\sigma$ than $dd\sigma$, $dd\pi$, and $dd\delta$. As we can see from Fig. 2, the deformation of the *s*-like QUAMBO from the free atomic orbital is more significant than the localized *d*-like QUAMBOs. Hence, the hopping integrals between the *d* orbitals are less prone to changes in the bonding environment due to their localized nature. Deviations of the hopping integrals from the two-center form are also observed in our previous study of Si.[29]

D. Orthogonal quasiatomic minimal basis orbitals

The QUAMBOs that we have constructed are only intra-atom orthogonal, i.e., the orbitals corresponding to the same atom are orthogonal, but orbitals corresponding to different atoms are not. The QUAMBOs can be constructed to be interatom orthogonal as well, and the effect of orthogonalization on the hopping integrals can be studied. By applying the symmetrical orthogonalization method, the Bloch wave function of each QUAMBO of all the atoms in the same unit cell can be made orthogonal to each other at a given $\mathbf{k}$,

$$\tilde{A}^{ortho}_{\mathbf{k},\alpha}(\mathbf{r}-\mathbf{R}_i)=\sum_{\alpha' i'}\tilde{A}_{\mathbf{k},\alpha}(\mathbf{r}-\mathbf{R}_i)[S(\mathbf{k})^{-1/2}]_{\alpha i,\alpha' i'}, \quad (14)$$

where $S(\mathbf{k})_{\alpha i,\alpha' i'}=\langle\tilde{A}_{\mathbf{k},\alpha}(\mathbf{R}_i)|\tilde{A}_{\mathbf{k},\alpha'}(\mathbf{R}'_i)\rangle$ and $\tilde{A}_{\mathbf{k},\alpha}(\mathbf{r}-\mathbf{R}_i)$ is the Bloch wave function of the QUAMBO that we obtained in Eq. (7). Since the Bloch wave functions of the QUAMBOs are orthogonal to each other at each $\mathbf{k}$ point in the Brillouin zone, the QUAMBOs obtained by

$$A^{ortho}_{\alpha}(\mathbf{r}-\mathbf{R}_i)=\sum_{\mathbf{k}}\tilde{A}^{ortho}_{\mathbf{k},\alpha}(\mathbf{r}-\mathbf{R}_i) \quad (15)$$

will be orthogonal not only to orbitals localized on the same atom but also to all the orbitals localized on atoms in other unit cells as well. The resultant orthogonal QUAMBOs are plotted in Figs. 9 and 10 for Mo in bcc and fcc structures, respectively. Except for the bcc *s* and d_{yz} QUAMBOs, all the other orthogonal QUAMBOs have part of their wave functions being pushed to neighboring atoms due to the imposed orthogonalization requirement. When compared to the QUAMBOs in Fig. 2, the orthogonal QUAMBOs appear tighter in general. However, the orthogonal QUAMBOs have considerable amplitude on neighboring atom sites and hence they are not necessarily more localized than the nonorthogonal

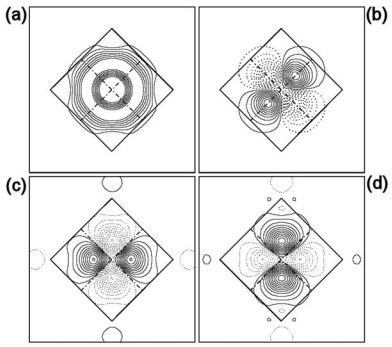

FIG. 9. Contour plot of the (a) *s*-like, (b) d_{yz}-like, (c) $d_{x^2-y^2}$-like, and (d) $d_{3z^2-r^2}$-like orthogonal QUAMBOs in bcc structure at equilibrium lattice constant. The values of the contour lines and indications of the neighbors' atomic positions are the same as in Fig. 2.

ones. We calculated the Slater-Koster hopping integrals for the orthogonal QUAMBOs and the results are plotted in Fig. 11. It can be noticed that the magnitude of the $ss\sigma$-, $sd\sigma$-, and $dd\sigma$-like hopping integrals are higher than that of the nonorthogonal QUAMBOs initially, but they decay faster as the interatomic distance increases, which is due to the more localized nature of the orthogonal QUAMBOs. Except for the $dd\pi$, there are sign changes in the orthogonal hopping integrals which can be attributed to some of the orthogonal orbital wave functions being pushed to neighboring atomic sites. In addition, since the orthogonal *d*-like QUAMBOs are now more deformed from the free atomic orbitals, there are more spread in the $dd\sigma$-, $dd\pi$-, and $dd\delta$-like hopping integrals when compared to Fig. 8.

According to Andersen's canonical band theory,[30,31] the hopping integrals for $dd\sigma$, $dd\pi$, and $dd\delta$ at the same interatomic distance should have a ratio of $-6:4:-1$. However, our results indicate that this canonical rule is not satisfied, although the relative signs are correct. We believe that this is due to the atomic sphere approximation being used by Andersen in which each atom is approximated by a spherically symmetric potential. From Figs. 2, 9, and 10, the deformation of the QUAMBOs indicates that the charge den-

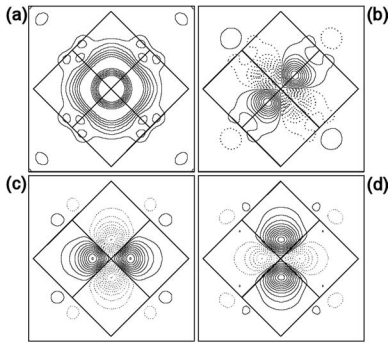

FIG. 10. Contour plot of the (a) *s*-like, (b) d_{yz}-like, (c) $d_{x^2-y^2}$-like, and (d) $d_{3z^2-r^2}$-like orthogonal QUAMBOs in fcc structure at equilibrium lattice constant. The values of the contour lines and indications of the neighbors' atomic positions are the same as in Fig. 2.

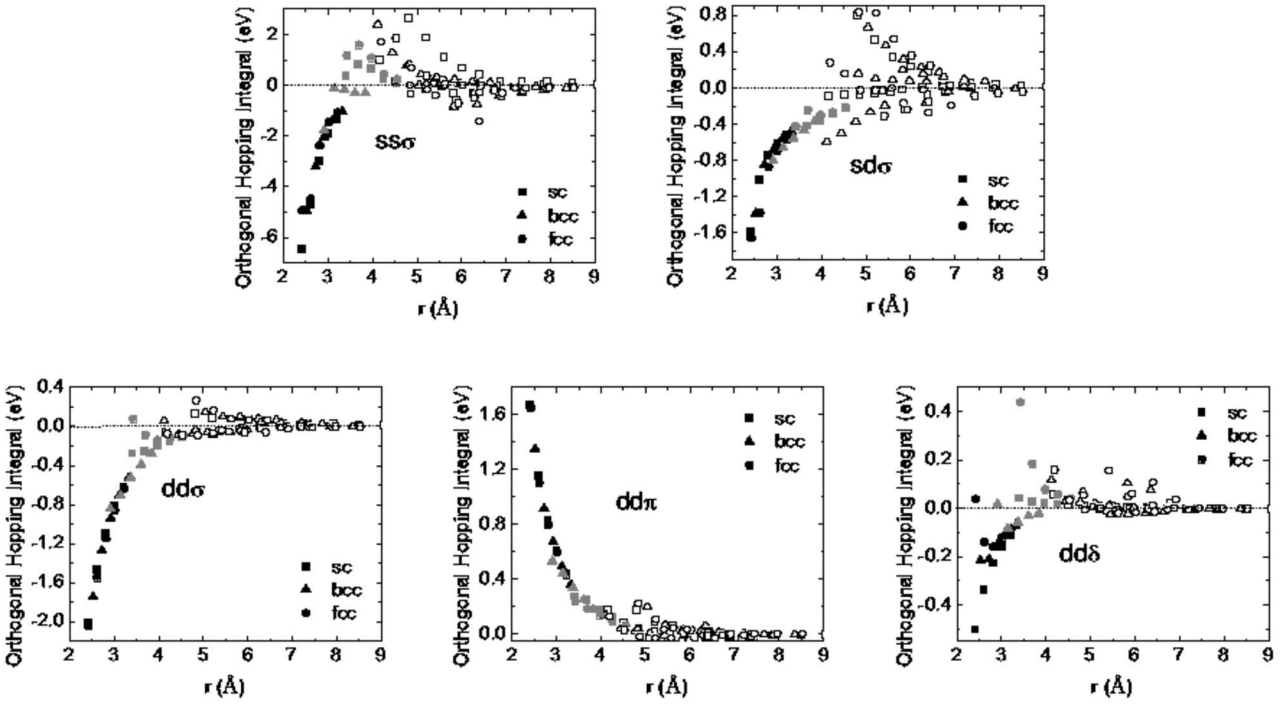

FIG. 11. Orthogonal hopping integrals for Mo as a function of interatomic distance in the bcc, fcc, and sc structures decomposed under the Slater-Koster tight-binding scheme. The black (gray) data points correspond to hopping integrals extracted from nearest (second nearest) neighbors, while the unshaded points correspond to third and further neighbors.

sity and the self-consistent potential is not spherically symmetric, resulting in deviations from the canonical theory.

IV. CONCLUSIONS

As a conclusion, we have constructed a minimal basis set of localized quasiatomic orbitals (QUAMBOs) for Mo in the bcc crystal structure by using the converged self-consistent eigenstates from first-principles calculations as input. The construction follows the procedure in Ref. 17, indicating that our method works for transition metals with localized *d* electrons in addition to the insulators and simple metals demonstrated in Ref. 17. The Mo QUAMBO basis reproduces all the occupied-state electronic properties of bcc-Mo. Moreover, population and bonding analysis can be made that provides interpretation based on chemical bonding, and we compared the Mulliken overlap population and bond order indices between bcc-Mo and fcc-Mo and between bcc-Mo, diamond-Si, and fcc-Al. The transferability of the two-center tight-binding models is also studied by using QUAMBO as a basis set; our results show that the two-center approximation is not adequate in describing the tight-binding hopping integrals.

ACKNOWLEDGMENTS

Ames Laboratory is operated for the U.S. Department of Energy by Iowa State University under Contract No. DE-AC02-07CH11358. This work was supported by the Director for Energy Research, Office of Basic Energy Sciences including a grant of computer time at the National Energy Research Supercomputing Center (NERSC) in Berkeley and Molecular Science Computing Facility (MSCF) in the Pacific Northwest Laboratory.

[1] L. Bytautas and K. Ruedenberg, Mol. Phys. **100**, 757 (2002).
[2] R. D. King-Smith and D. Vanderbilt, Phys. Rev. B **47**, 1651 (1993).
[3] R. Resta, Rev. Mod. Phys. **66**, 899 (1994).
[4] G. Galli and M. Parrinello, Phys. Rev. Lett. **69**, 3547 (1992).
[5] F. Mauri, G. Galli, and R. Car, Phys. Rev. B **47**, 9973 (1993).
[6] P. Ordejon, D. A. Drabold, M. P. Grumbach, and R. M. Martin, Phys. Rev. B **48**, 14646 (1993).
[7] J. Kim, F. Mauri, and G. Galli, Phys. Rev. B **52**, 1640 (1995).
[8] E. Hernandez and M. J. Gillan, Phys. Rev. B **51**, 10157 (1995).
[9] G. H. Wannier, Phys. Rev. **52**, 191 (1937).
[10] W. Kohn, Phys. Rev. B **7**, 4388 (1973).
[11] L. He and D. Vanderbilt, Phys. Rev. Lett. **86**, 5341 (2001).
[12] N. Marzari and D. Vanderbilt, Phys. Rev. B **56**, 12847 (1997).
[13] G. Berghold, C. J. Mundy, A. H. Romero, J. Hutter, and M. Parrinello, Phys. Rev. B **61**, 10040 (2000).
[14] P. L. Silvestrelli, Phys. Rev. B **59**, 9703 (1999).
[15] A. Shukla, M. Dolg, P. Fulde, and H. Stoll, Phys. Rev. B **57**, 1471 (1998).
[16] I. Souza, N. Marzari, and D. Vanderbilt, Phys. Rev. B **65**, 035109 (2001).
[17] W. C. Lu, C. Z. Wang, T. L. Chan, K. Ruedenberg, and K. M. Ho,

Phys. Rev. B **70**, 041101(R) (2004).
[18] D. Vanderbilt, Phys. Rev. B **41**, 7892 (1990); K. Laasonen, R. Car, C. Lee, and D. Vanderbilt, *ibid.* **43**, 6796 (1991); K. Laasonen, A. Pasquarello, R. Car, C. Lee, and D. Vanderbilt, *ibid.* **47**, 10142 (1993).
[19] P. E. Blochl, Phys. Rev. B **50**, 17953 (1994).
[20] X. F. Qian, J. Li, T.-L. Chan, Y. X. Yao, C.-Z. Wang, K.-M. Ho, and S. Yip (unpublished).
[21] P. Hohenberg and W. Kohn, Phys. Rev. **136**, B864 (1964); W. Kohn and L. J. Sham, *ibid.* **140**, A1135 (1965).
[22] C.-L. Fu and K.-M. Ho, Phys. Rev. B **28**, 5480 (1983).
[23] S. G. Louie, K.-M. Ho, and M. L. Cohen, Phys. Rev. B **19**, 1774 (1979).
[24] H. J. Monkhorst and J. D. Pack, Phys. Rev. B **13**, 5188 (1976).
[25] If the transformation is done regardless of the singularity, the resultant QUAMBOs will lead to the unphysical Mulliken overlap population and bond order analysis in Sec. III B.
[26] R. S. Mulliken, J. Chem. Phys. **23**, 1833 (1955).
[27] I. Mayer, Chem. Phys. Lett. **97**, 270 (1983).
[28] J. C. Slater and G. F. Koster, Phys. Rev. **94**, 1498 (1954).
[29] W. C. Lu, C. Z. Wang, K. Ruedenberg, and K. M. Ho, Phys. Rev. B **72**, 205123 (2005).
[30] O. K. Andersen, Phys. Rev. B **12**, 3060 (1975).
[31] D. G. Pettifor, J. Phys. C **5**, 97 (1972); D. G. Pettifor, J. Phys. F: Met. Phys. **7**, 613 (1977).